Journal of the Indian Institute of Science
A Multidisciplinary Reviews Journal
ISSN: 0970-4140 Coden-JIISAD

REVIEWS

Plasmonic Microstructured Optical Fibers and Their Application in Bio-Sensing

*Tushar Biswas, Rik Chattopadhyay and Shyamal K. Bhadra**

Abstract | Microstructured optical fiber embedded with metallic thin wire has been widely used for bio-sensing based on the principle of surface plasmon resonance. We review and study the fundamental properties like operating principle, design and performance of plasmonic microstructured optical fiber following photonic band gap theory. Finally, we present a very simple design of metal embedded hollow-core photonic crystal fiber for efficient sensing of very low refractive index, which can find potential application in bio-sensing.

1 Introduction

Development of sensors for low Refractive Index (RI) sensing has seen tremendous research interest for their possible application in bio-sensing. Various RI sensors based on conventional optical fibers and microstructured optical fibers (MOFs) have been reported.[1–11] Many of them utilize the phenomenon of Surface Plasmon Resonance (SPR). Unlike the bulk Kretschmann-Raether model, these sensors are very compact and possess remote sensing capabilities. Another advantage of plasmonic MOF based sensors is that they can be integrated with large microfluidic channels owing to its micro-size. The analyte channels are coated with a metal to generate Surface Plasmons (SPs) in some of the MOF based sensors. Difficulty with fabricating these sensors is that they require metal coating of precise thickness in nanometer scale. This difficulty can be overcome by using metal wire filled MOF to generate SPs.[12]

SPs are highly sensitive to the changes in the surrounding dielectric medium. Thus, one launches light into the core of the plasmonic MOF and probes the change in neighbouring analyte by observing the change in coupling between the core-guided mode and the SP mode. Efficient coupling requires the establishment of phase matching condition between the core guided mode and the SP mode. Therefore, in designing low RI senors, difficulties arise due to the fact that it requires low effective index of core guided mode. Gauvreau et al.[5] proposed plasmonic Photonic Band Gap Fiber (PBGF) based sensors to overcome the problem. However, these designs are very tricky and may be difficult to fabricate. We explore the possibility of SPR based RI sensing effect in conventional Hollow-Core Photonic Crystal Fiber (HC-PCF), which is a special type of MOF containing periodic arrangement of air holes in silica host. Air-holes of the cladding of the HC-PCF can be selectively replaced by silver wire to generate SPs. The material whose index is to be sensed can be filled into the core of the fiber. Practically, the proposed fiber can be fabricated by incorporating Taylor-wire process[13] in the conventional stack and draw method. Generally, metal-wires are integrated with PCFs using a high-temperature pressure cell approach to pump molten silver and gold into the hollow channels of PCFs.[14–16]

We present the design of a HC-PCF operating at a centre wavelength of 1550 nm. This fiber can guide light through the core either by Bragg's reflection, or by Modified Total Internal Reflection (MTIR), depending on the RI value of the core filling material. The band structure of HC-PCF is calculated using Plane Wave Expansion Method (PWEM),[17] and the propagation characteristics of the analyte-filled fibers is simulated through the Finite Element Method (FEM)[18] based COMSOL-Multiphisics software. We found that the HC-PCF with pitch (Λ) value of 2.74 microns and air hole diameter (d) of 2.603 microns have effective index of the fundamental space filling mode (n_{FSM}) less than 1.2 in the wavelength range 1300–1700 nm. This fiber is utilized to obtain low effective index of the core guided mode. The air holes of the same fiber are then selectively replaced by silver to

Fiber Optics & Photonics Division, CSIR-Central Glass & Ceramic Research Institute, Jadavpur, Kolkata 700032, India.
**skbhadra@cgcri.res.in*

generate SPs. We vary the value of RI of the core according to the value of RI of bio-analyte. Next we study the propagation characteristics of the analyte-filled fiber. The absorption loss spectra show that wavelength of peak absorption due to SPR alters with the change in the value of core RI. A sensitivity curve is obtained by plotting the shift in the resonant wavelength against the analyte index. Finally, we present a discussion on numerical results and conclude by summarizing the major findings.

2 Design of HC-PCF with Low Effective Core Index

The effective index of the fundamental core guided mode of a HC-PCF can be tuned by changing the core filling material. The light guidance mechanism can be switched from Bragg's reflection to MTIR by increasing the core RI value beyond the n_{FSM}.[19,20] In this section, we present the design of a HC-PCF which has a core effective index as low as 1.22 operating in the wavelength region 1300–1700 nm. The unfilled HC-PCF guides the light into the air core by trapping the electromagnetic modes which are forbidden to propagate through the intrinsic photonic crystal (PC) cladding. One has to calculate the photonic band structure (PBS) to determine the operating wavelength region of the HC-PCF. The schematic diagram of a hexagonal unit cell of defect less PC cladding is shown in Figure 1.

The PBS of such cladding can be calculated by solving Maxwell's wave equations as given by

$$\nabla\times\left[\nabla\times E(x\,|\,\omega)\right]=\frac{\omega^2}{c^2}\varepsilon(x_{\|})E(x\,|\,\omega) \qquad (1)$$

$$\nabla\times\left[\nabla\times H(x\,|\,\omega)\right]=\frac{\omega^2}{c^2}\varepsilon(x_{\|})H(x\,|\,\omega) \qquad (2)$$

where $\boldsymbol{E}(\boldsymbol{x}|\omega)$ and $\boldsymbol{H}(\boldsymbol{x}|\boldsymbol{\omega})$ are electric and magnetic fields respectively, c is the velocity of light in free space, and $\varepsilon(\boldsymbol{x}_{\|})$ is the periodic dielectric permittivity defining the PC cladding. One has to solve either one of the equations to obtain the PBS of the cladding. We solve Eq. (1) by using PWEM. In this method the periodic dielectric function is expanded through Fourier series sum, while the periodic solution of the electric or magnetic is expressed by Bloch-Floquet theorem to substitute them into Eq. (1) or (2). This reduces the problem to a system of eigen value matrix equations, which is further solved by matrix diagonalization method. The plot of the eigen frequency as a function of the wave vector is known as PBS. The real value eigen solutions (eigen frequencies) are only permitted to propagate through the PC cladding. The complex valued solutions are forbidden to propagate through the cladding. Hence, they form the Photonic Band Gap (PBG). Electromagnetic modes having these values of frequencies can be trapped into the air core. The centre wavelength and bandwidth of a HC-PBGF for a constant dielectric contrast between air and the host material depends on Λ and d. So the desired wavelength of operation can be obtained by varying d and Λ. Numerical calculations show that the centre wavelength of a HC-PCF is red shifted with the increase in Λ, and the bandwidth decreases with the decrease in air filling fraction, which is defined by the ratio of d to Λ. After several iterations and considering the optimized experimental

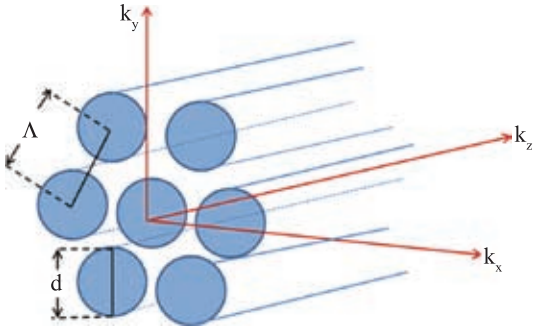

Figure 1: Schematic diagram of hexagonal unit-cell of a defect less PC cladding.

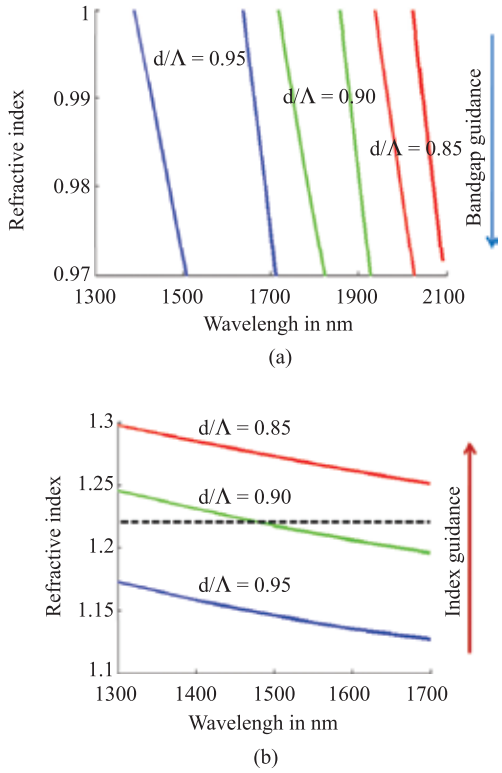

Figure 2: (a) Variation of PBG and (b) effective cladding index with air filling fraction.

conditions, the value of Λ is fixed to 2.74 microns. The variations of PBG and n_{FSM} for a fixed value of Λ = 2.74 microns and varying air filling fraction (d/Λ) are shown Figures 2(a) and (b) respectively.

We can see from this figure that for an air filling fraction of 95%, the fiber with air core has a centre wavelength of 1550 nm and the value of n_{FSM} lies below 1.2 in the wavelength range of 1300–1700 nm. Therefore, the HC-PCF having such structural parameters can guide light through 1500 nm to 1650 nm by Bragg's reflection with $n_{core} = 1$ and through 1300 nm to 1700 nm with $n_{core} > 1.2$ by MTIR. The schematic diagram of HC-PCF with Λ = 2.74 and d = 2.603 is shown in Figure 3, with two HC-PCFs. Small and large core HC-PCF can be designed by removing 7 and 19 central air capillaries respectively from the hexagonal stack of pure silica capillaries.

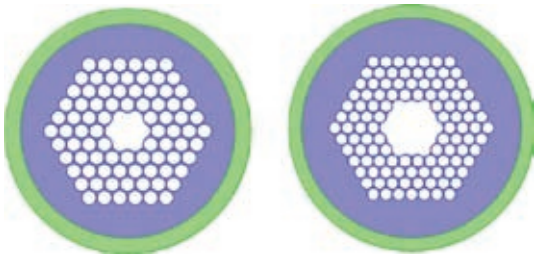

Figure 3: Schematic diagram of (a) small and (b) large core HC-PCF. The white circle and the regions shaded in blue and green colours represent the air holes and host silica and perfectly matched layer respectively.

We study the propagation characteristics of these fibers using FEM (COMSOL-Multiphysics). Numerical simulations confirm that the unfilled small or large core HC-PCFs have band limited transmission characteristics, as is illustrated in Figure 4(a). In this figure the region bounded by the dashed lines represents the PBG calculated by PWEM which is further verified by FEM, and the results are shown in red dots. The blue and red lines represent the dispersions of the fundamental core guided modes of the small and large core HC-PCFs respectively. The effective indices lie below the unity in both the cases, since light is guided through air. In this way light can be guided through the core by

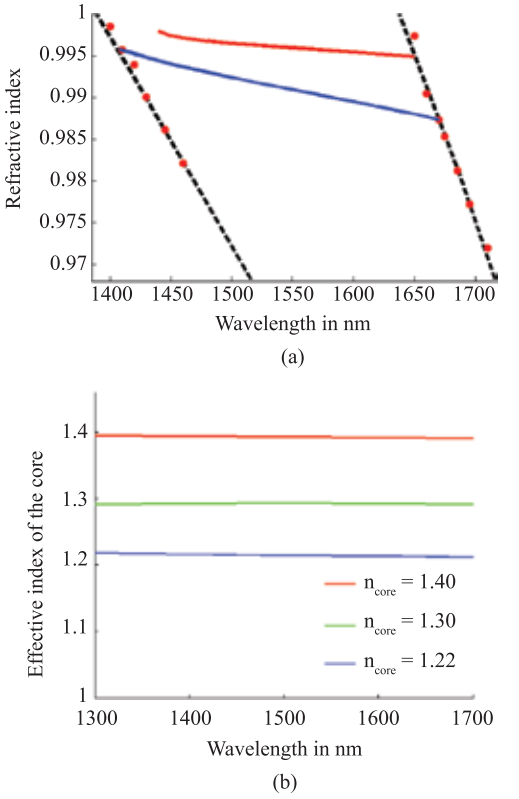

Figure 4: (a) The out-of-plane band gap of the PC cladding (dashed lines and red dots represent the results obtained by PWEM and FEM respectively). The blue and red curves represent the dispersion of the fundamental modes of the small and large core HC-PBGF respectively. (b) Dispersions of fundamental core guided modes with various core analytes.

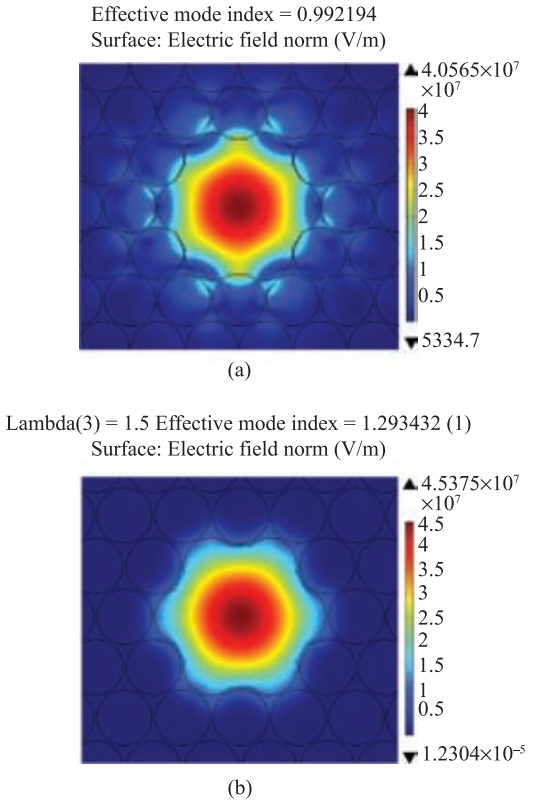

Figure 5: The fundamental mode field distribution for (a) $n_{core} = 1$ and $n_{core} = 1.3$ at a wavelength of 1500 nm.

Bragg's reflection for value of core RI smaller than n_{FSM}. Now if one replaces the core analytes of RI values higher than that of the n_{FSM}, the same fibers would guide light by MTIR. In this case the transmission is no more restricted within the bandgap region, which is also evident from the simulations. The dispersions of the fundamental core guided modes for various core filling analytes having different indices are shown in Figure 4(b).

The fundamental mode field distribution of the unfilled air core and with core filling analyte RI value of 1.3 at operating wavelength of 1500 nm are shown in Figures 5(a) and (b) respectively.

3 Surface Plasmon Resonance in Metal Filled HC-PCF

In this section we investigate the transmission properties of metal filled HC-PCF. One has to first study the Surface Plasmon Polariton (SPP) generated on a single metal wire embedded in an otherwise defectless PC as shown in Figure 6(a) in order to understand the propagation characteristics of metal filled HC-PCF. So, initially we study the transmission property of the structure shown in Figure 6(a), and then we focus our attention to the structure shown in Figure 6(b) in which one of the air holes of the cladding of the HC-PCF is replaced by silver wire.

The value of RI of the core filling material is assumed to be 1.3 in this particular case. We have used Sellmeier equation[21] for dispersion of silica, and Lorentz-Drude model[22] for silver. Analytically, the expression for the wave vector associated with SPP can be written as the equation[23]

$$k_{SPP} = \frac{2\pi}{\lambda}\sqrt{\frac{\varepsilon_s \varepsilon_m}{\varepsilon_s + \varepsilon_m} - \left(\frac{(n-1)\lambda}{d\pi}\right)^2} \qquad (3)$$

where λ is the free space wavelength, d is the diameter of the metal wire, and ε_s and ε_m are the dielectric permittivities of the surrounding medium and metal respectively. It can be noticed from Eq. (3) that various SPP modes can be generated on metal wire for different values of n. The dispersions of $n = 3$ and $n = 4$ SPP modes are shown in red lines in Figure 7(a).

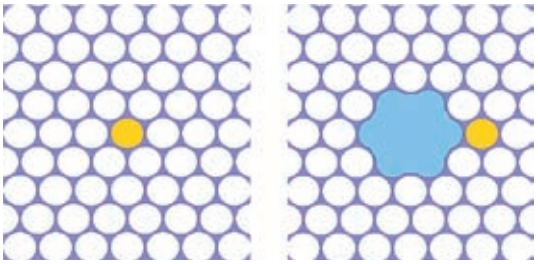

(a) (b)

Figure 6: (a) Single metal wire in a PC. (b) Single metal wire in an analyte filled HC-PCF. Yellow circles in this figure represent the metal wire.

We use the structure as shown in Figure 6(b) in FEM simulation. The mode analysis of the structure gives us the effective indices of the various SPP coupled core guided modes. The dispersion of the SPP coupled fundamental core guided mode is shown in blue line in Figure 7(a). Figure 7(b) shows the attenuation of the SPP coupled core guided mode. In this figure we can see two absorption peaks. Such absorption peaks are generated due to resonant coupling between the core guided mode and the two SPP modes. Expression for the wave vector associated with core guided mode can be written as the equation

$$k_z = kn_{\text{core}} \sin\theta = \frac{2\pi}{\lambda} n_{\text{core}} \sin\theta \qquad (4)$$

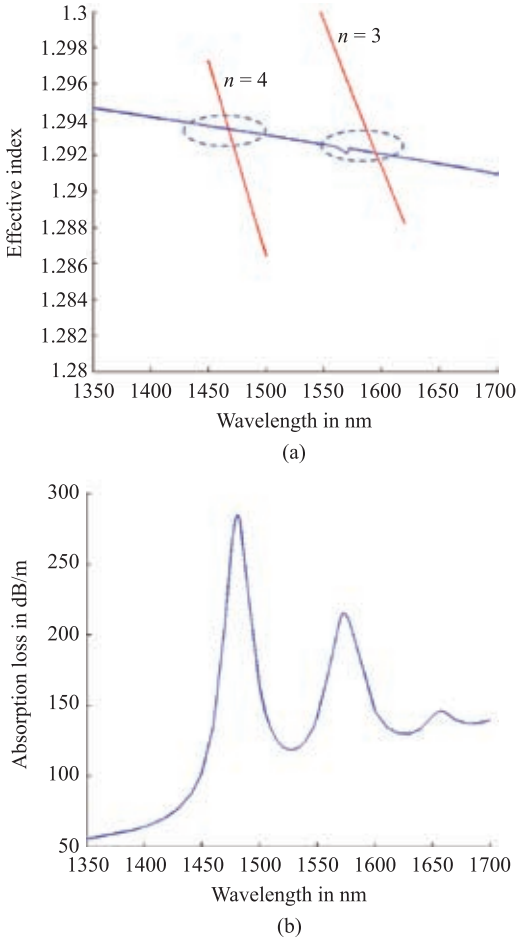

Figure 7: (a) Dispersions of various SPP modes (red lines) and SPP coupled core guided mode (blue line). (b) Absorption loss spectrum of the SPP coupled core guided mode.

where k is the in plane wave vector, n_{core} is the refractive index of the core, θ is the angle between the in-plane wave vector and the incident wave vector, and λ is the operating wavelength. When light is launched into the core of the HC-PCF, as shown in Figure 6(b), SPs are generated on the surface of metal wire. SPR occurs when the phase matching condition between the core guided mode and the SPP mode is established. Mathematically, the phase matching is achieved by equating Eqs. (3) and (4). From Eq. (3) we can see that various SPP modes can be generated on the metal wire for different values of n. These SPP modes anti-cross with the fundamental core guided mode. Thus, several absorption peaks are obtained at various wavelengths because of anti-crossing of various SPP modes with the core guided mode. We notice from Figure (7) that there is a shift between the anti-crossing wavelength and peak absorption wavelength. This is due to the fact that while calculating the dispersion of SPP modes we consider defectless PC. The effective index of neighbouring medium of the metal wire changes due to analyte filling into the core of the HC-PCF. The electric field distribution of the SPP mode with n = 3 and the SPP coupled fundamental core guided mode are shown in Figures 8(a) and (b) respectively.

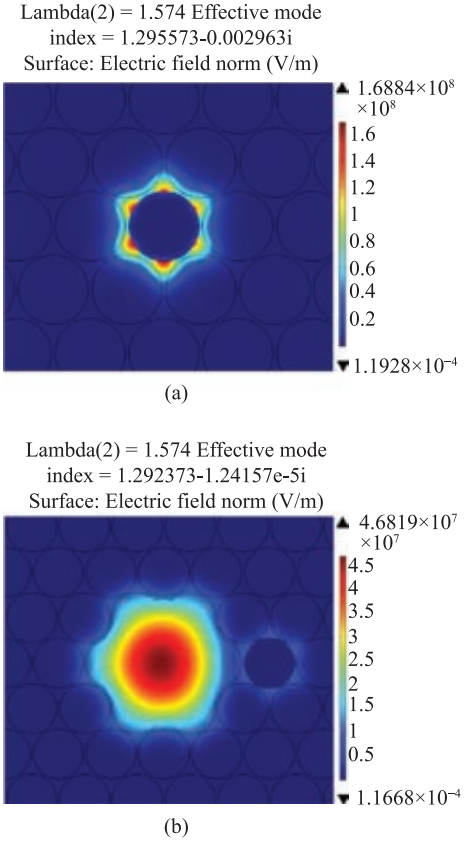

Figure 8: Electric field distribution of (a) n = 3 SPP mode and (b) SPP coupled fundamental core guided mode at the SPR wavelength of 1574 nm.

4 Effect of the Number of Metal Wires and Their Orientation

SP coupling depends on the number of metal wires and their orientation in the cladding. Primarily we replace one of the air holes in the first layer of cladding by silver, which is shown in the inset of Figure 9(a). In this figure we have shown the loss spectra of the structure for two different core RI values of 1.3 and 1.302 respectively; it shows two sensitive absorption peaks. We observed that using one metal wire coupling of SPP with core guided mode is only possible when the metal wire is placed in the first ring. Later we study the SPP coupling property using two metal wires. Three different combinations of two metal wires are shown in Figures 9(b), (c) and (d) respectively. Two metal wires are placed into two consecutive holes in both combinations of Figures 9(b) and (c), the difference is that in the former case the wires are placed in the first ring of the air holes, whereas in the latter case they are place in the first and second ring respectively.

Placing several metal wires in the cladding reveals that their orientation is very important. In case of two metal wires placed into the first layer of holes, the loss of the core guided mode is enhanced due to the proximity of metal wires closer to the core. Only one high absorption peak is observed when the two metal wires are placed into the different layers of holes, while two high absorption peaks are seen for two wires placed into the first layer. In case of the structure shown in Figure 9(d) where two metal wires are placed into the first ring of the holes, provided the separation between them is maximum, the loss spectra are similar to that of the structure shown in Figure 9(a). In this case the loss is enhanced due to increase in the number of metal wires. We notice that the absorption peaks are red shifted with the increase in indices of the core analytes. It can be seen that the whole spectra are blue shifted in Figures 9(b) and (c). Then we replace all the air holes of the first ring of the cladding of small and large core HC-PCF which are shown in the insets of Figures 9(e) and (f). These figures show two resonant absorption peaks in the same wavelength range for core analyte index as low as 1.24. Therefore these two structures can be utilized to detect very low RI of any fluid. The loss spectra of the structures containing several metal wires placed close to each other are different from that of the structure containing one metal wire, because in the former cases the core guided modes

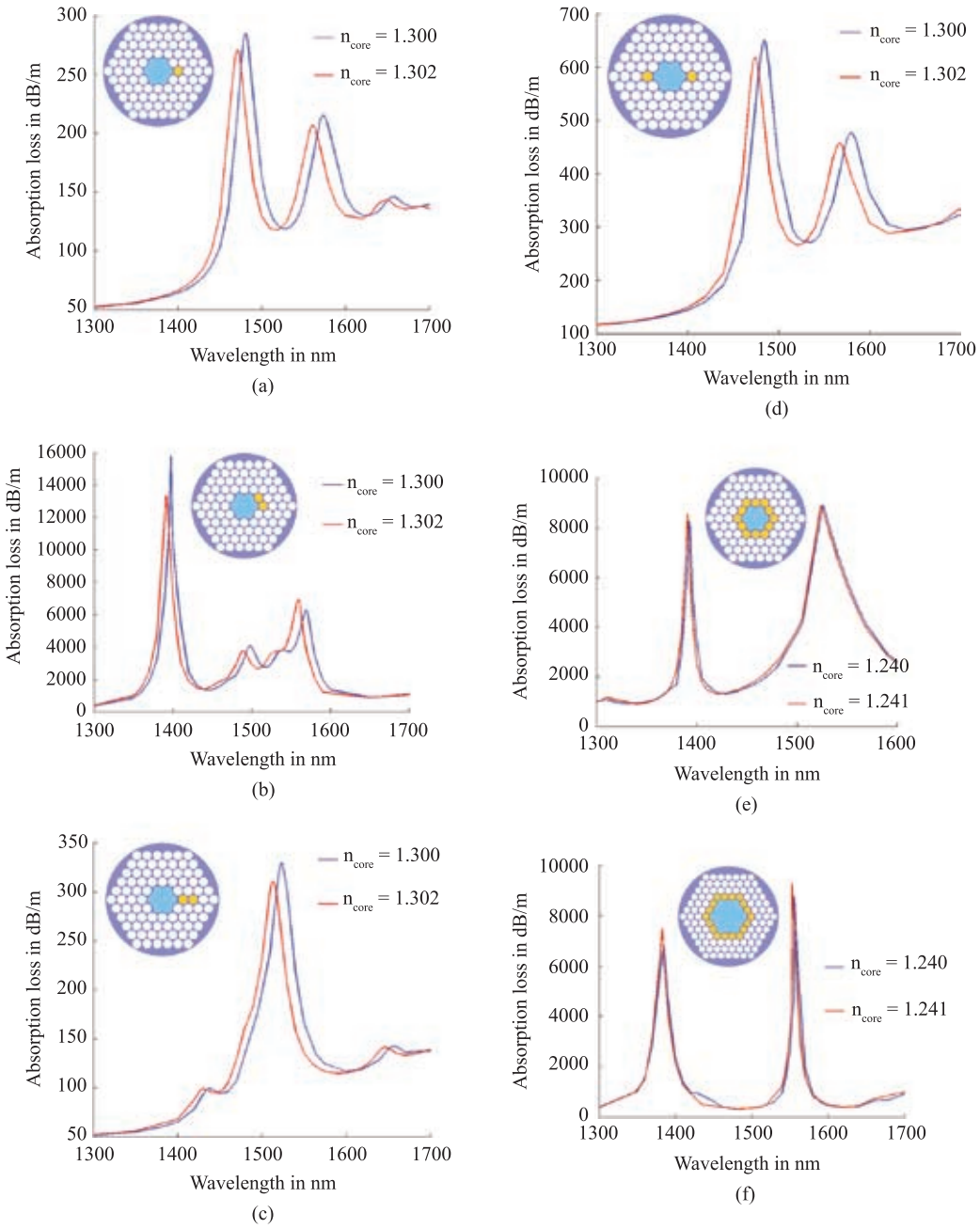

Figure 9: Absorption loss spectra of various combinations of metal wires in the cladding.

are coupled with the SPP super-modes that are combinations of SPP modes generated on a single metal surface.

5 Sensing Principle

In the previous section we have seen that the absorption loss peaks shift with the change in core analyte RI value. It is also evident from Eqs. (3) and (4) that the numerical value of wave vectors of fundamental core guided mode and SPP mode varies with the change in core analyte RI. Therefore, the SPR wavelength shifts with the change in core analyte RI value. The shift of SPR wavelength with core analyte can be utilized to design RI sensor using these fibers. The loss spectra for different values of RI of core filling are calculated to measure the amount of wavelength shift. The value of unknown analyte can be predicted from the sensitivity plot, which can be obtained by plotting the SPR wavelengths as a function of

core analyte RI. The spectral sensitivity can be defined by the equation

$$S_\lambda[nmRIU^{-1}] = \frac{d(\lambda_{\text{peak}}(n_a))}{dn_a} \quad (5)$$

where S_λ is the spectral sensitivity measured in nm per unit change in RI, λ_{peak} is the SPR wavelength, and dn_a represents the differential change in core analyte RI. Generally, the spectral sensitivity is obtained by calculating the slope of the n_a versus λ_{peak} plot.

6 Results and Discussion

The variations of first resonant wavelength with core RI value of four selected structures are shown in figure 10.

We calculated sensitivity of HC-PCFs with various combinations of metal wires in the cladding. We chose the results of four combinations that are shown in Figures 9(a), (d), (e) and (f), and designated them as Type I, II, III and IV respectively. It can be noticed from Figure 10 that the sensitivity curves are almost linear. The sensitivities obtained by calculating the slopes of the sensitivity curves from various structures are shown in Table 1.

The maximum sensitivity of 6673 nmRIU^{-1} is achieved with the structure as shown in Figure 9(d). Sensitivity of the second peak is higher than that of the first peak. Though Types III and IV show smaller sensitivities, the novelty is that they can detect very low value of RI liquids, such as bio-fluids.

Table 1: Sensitivities of various HC-PCFs.

Fiber type	Sensitivity (nm.RIU^{-1})	
	Peak 1	Peak 2
I	5310	6612
II	5389	6673
III	1750	2000
IV	1569	2151

7 Conclusions

In this study we have shown the utilization of hollow core photonic bandgap fiber as low RI sensor. A conventional HC-PCF with selective metal filled air hole is sensitive towards the change in core RI. We studied the effect of metal wire filled air hole on the core guided mode. It is revealed that the number of metal filled air-holes is important to specify the range of refractive index that could be sensed with the help of this kind of fiber. The orientation of metal filled air-hole is important to vary the sensitivity towards core RI.

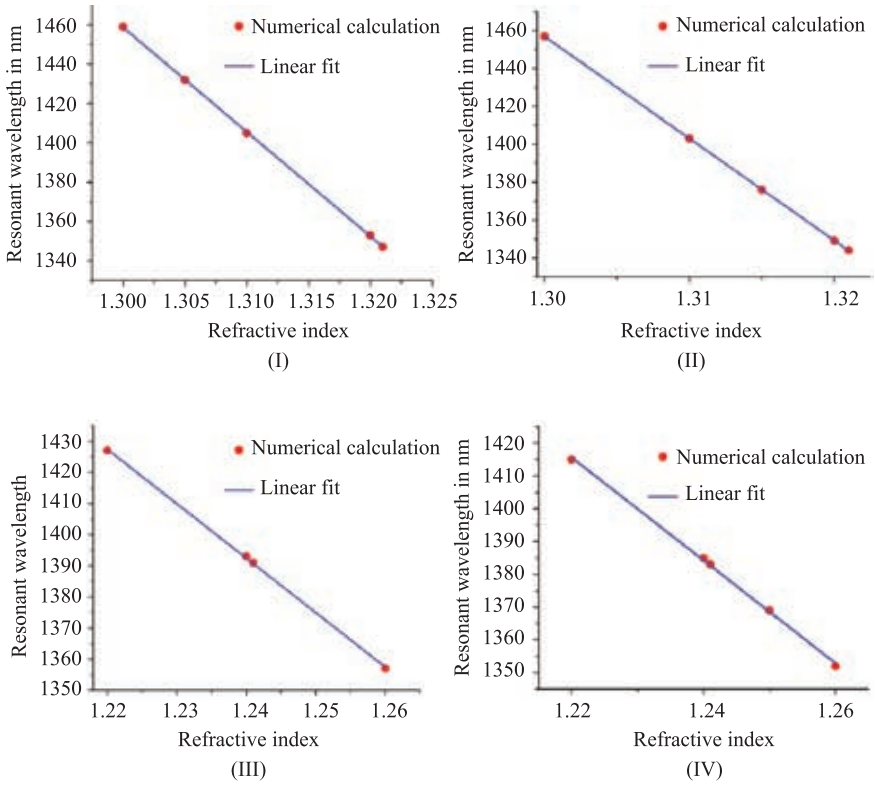

Figure 10: Variations of resonant wavelength with core analyte RI.

The study shows that we can achieve maximum sensitivity when two diagonally opposite air holes are filled with metal. On the other hand, if one wishes to sense low value of RI, then all the air holes in the first ring should be filled with metal, though sensitivity gets reduced. Therefore, it is expected that the structure responds to low RI at the expense of sensitivity; similarly, the sensitivity can be increased but the structure responds only at higher values of RI. Hence, there is a scope to develop new type of HC-PCFs using conventional methods, which can trade off between these two extremities.

Acknowledgements

The authors acknowledge The Director, CSIR-CGCRI for support and encouragement to carry out this work. Author TB acknowledges CSIR 12th five-year-plan project—GLASSFIB for funding this work. Author RC acknowledges CSIR for senior research fellowship. The authors are grateful to all the staff members of FOPD, CSIR-CGCRI, for their help.

Received 11 June 2014.

References

1. J. Homola, "Optical fiber sensor based on surface Plasmon excitation", *Sensors and Actuators B*, 29, 401–405.
2. Hassani and M. Skorobogatiy, "Design of the Microstructured optical fiber-based surface plasmon resonance sensors with enhanced microfluidics", *Opt. Express*, 14, 11616–11621.
3. A. Hassani and M. Skorobogatiy, "Design criteria for microstructured-optical-fiber based surface-plasmon-resonance sensors", *J. Opt. Soc. Am. B,* 26, 1423–1428.
4. A. Hassani, B. Gauvreau, M. F. Fehri, A. Kabashin and M. Skorobogatiy, "Photonic crystal fiber and waveguide-based surface plasmon resonance sensors for application in the visible and near-IR", *Electromagnetics*, 28, 198–213.
5. B. Gauvreau, A. Hassani, M. F. Fehri, A. Kabashin, M. Skorobogatiy, "Photonic bandgap fiber-based Surface Plasmon Resonance sensors", *Opt. Express*, 15, 11413–11426.
6. A. Hassani and M. Skorobogatiy, "Photonic crystal fiber-based plasmonic sensors for the detection of biolayer thickness", *J. Opt. Soc. Am. B*, 26, 1550–1557.
7. X. Yu, Y Zhang, S. Pan, P. Shum, M. Yan, Y. Leviatan and C. Li, "A selectively coated photonic crystal fiber based surface plasmon resonance sensor", *J. Opt.* 12, 015005.
8. B. Shuai, L. Xia, Y. Zhang, and D. Liu, "A multi-core holey fiber based plasmonic sensor with large detection range and high linearity", *Opt. Express*, 20, 5975–5986.
9. G. E. Town, W. Yuan, R McCosker O. Bang "Microstructured optical fiber refractive index sensor", *Optics Letters,* 35(6), 856–858.
10. Z. Pei-pei, Y. Jian-quan, C. Hai-xia, and L. Ying, "A surface plasmon resonance sensor based on a multicore photonic crystal fiber", *Optoelectronics letters,* 9, 0342.
11. Y. Lu, C. J. Hao, B. Q. Wu, M. Musideke, L. C. Duan, W. Q. Wen and J.Q. Yao, "Surface Plasmon Resonance Sensor Based on Polymer Photonic Crystal Fibers with Metal Nanolayers", *Sensors* , 13, 956–965.
12. X. Fu, Y. Lu, X. Huang, C. Hao, B. Wu, J. Yao, "Surface plasmon resonance sensor based on photonic crystal fiber filled with silver nanowires", *Optica Applicata* XLI, 941–951.
13. G. F. Taylor, "A method of drawing metallic filaments and a discussion of their properties and uses", *Phys. Rev.* 23, 655–660.
14. M. A. Schmidt, L. N. P. Sempere, H. K. Tyagi, C. G. Poulton and P. S. J. Russell, "Wave guiding and plasmon resonances in two-dimensional photonic lattices of gold and silver nanowires" *Phys. Rev. B* 77, 033417.
15. J. Hou, D. Bird, A. George, S. Maier, B. T. Kuhlmey, and J. C. Knight, "Metallic mode confinement in microstructured fibres", *Opt. Express* 16, 5983–5990.
16. H. W. Lee, M. A. Schmidt, H. K. Tyagi, L. P. Sempere and P. St. J. Russell,(Check) "Polarization-dependent coupling to plasmon modes on submicron gold wire in photonic crystal fiber", *Applied Physics Letters* 93, 111102.
17. A. Maradudin, "Out of plane propagation of electromagnetic waves in a two dimensional dielectric medium", *J. Mod. Opt.* 41, 275–284.
18. K. Saitoh and M. Koshiba, "Full-vectorial imaginary-distance beam propagation method based on finite element scheme: Application to photonic crystal fibers", *IEEE J. Quantum Electron.* 38, 927–933.
19. P. Russell, "Photonic crystal fibers", Science 299, 358–362.
20. F. Benabid, "Hollow-core photonic bandgap fibre: New light guidance for new science and technology", *Phil. Trans. R. Soc. A*, 364, 3439–3462.
21. G. P. Agrawal, "Nonlinear Fiber Optics", Academic Press, San Diego, CA, 1989.
22. A. D. Rakić, A. B. Djurišic, J. M. Elazar, and M. L. Majewski, "Optical properties of metallic films for vertical-cavity optoelectronic devices", *Applied Optics*, 37(22), 5271–5283.
23. M. A. Schmidt and P. S. J. Russell, "Long-range spiralling surface plasmon modes on metallic nanowires", *Opt. Express*. 16, 13617–13623.

Tushar Biswas received M.Sc. in Electronics from West Bengal State University, India in 2011. He is perusing Ph.D. under the supervision S.K. Bhadra in the fiber optics and photonics division, CSIR-Central Glass and Ceramic Research Institute, Kolkata, India. He has been engaged in research on hollow-core photonic band gap fiber, plasmonics and metamaterials.

Rik Chattopadhyay is a senior research fellow (CSIR-SRF) in CSIR-Central Glass and Ceramic Research Institute, Kolkata, India and is pursuing his Ph.D. work under Dr. S.K. Bhadra. He received his B.Sc. (Hons.) in physics from University of Calcutta, India. He also received B. Tech and M. Tech in Optics and Optoelectronics from same university. His current research interest is on nanoplasmonics and metamaterial devices for optical communication and medical appliances.

Shyamal Kumar Bhadra is a Chief Scientist at CSIR-Central Glass and Ceramic Research Institute, Kolkata, India, where he is currently involved in the advanced areas of fiber optics and photonics. He has coordinated various national and international research projects and published more than 100 research papers in international reputed journals. He is the holder of five national and international patents. He is the Honorary Editor of the Journal of Transaction Indian Ceramic Society since 2006. His research interests include fiber laser, photonic crystal fiber & supercontinuum generation, nonlinear optics & ultrafast pulse dynamics in guided medium and plasmonics metamaterials. He took the leadership role for commercialization of two photonic products in India-Erbium Doped Fiber Amplifier (EDFA) and broadband super continuum light source. He received the best technology award along with his group of CSIR-Plan-project in 2012.